Energy Proceedings
Vol 60, 2025
ISSN 2004-2965

Dynamic Identification and Prediction of a Marine Parallel IRGT/SOFC Hybrid System Using LSTM Network#

Jiale Wen[1], Shengying Xiao[1], Xicong Mi[1], Catalina Spataru[2], Yiwu Weng[3], Xiaojing Lv[1*]

1 China-UK Low Carbon College, Shanghai Jiao Tong University, Shanghai, 201306, China

2 Energy Institute, University College London, London, WC1H0NN, United Kingdom

3 School of Mechanical Engineering, Shanghai Jiao Tong University, Shanghai,200240, China
*(Corresponding Author: lvxiaojing@sjtu.edu.cn)

ABSTRACT

In response to the frequent faults and low efficiency caused by response delay and power imbalance in dual-unit intercooled reheat gas turbine/solid oxide fuel cell (IRGT/SOFC) hybrid systems under multiple operating scenarios, this study proposes a multi-input multi-output (MIMO) long short-term memory (LSTM) neural network for dynamic identification and prediction. By integrating physics-based modeling with data-driven training, the proposed framework captures the transient behaviors of a marine parallel IRGT-SOFC system across varying fuel scenarios. Sensitivity analyses on sampling rate, hidden layer configuration, and learning rate demonstrate that a single-layer LSTM with 50 neurons and 0.01 s sampling interval provides the optimal balance between prediction accuracy and computational cost. The trained model achieved R^2 values exceeding 0.998 across all key outputs, with MAPE consistently below 0.79% except T_{FCavg} , effectively predicting power output, SOFC temperature, and overall system efficiency. The proposed model effectively captures the transient response patterns of dual-unit systems under varying fuel input, laying a high-precision modeling foundation for predictive power control of next-generation marine propulsion systems in complex operational scenarios.

Keywords: All-electric propulsion system; Dual unit IRGT/SOFC; MIMO-LSTM; Real-time prediction

NONMENCLATURE

Abbreviations	
IRGT	Intercooled reheat gas turbine
IPS	Integrated power system
LPC	Low-pressure compressor
HPC	High-pressure compressor
CC	Combustion chamber
HPT	High-pressure turbine
LPT	Low-pressure turbine
PT	Power turbine
HE	Heat exchanger
CCC	Catalytic combustion chamber
P-R	Pre-reformer
CR	Cracker
G	Generator
TIT	Turbine inlet temperature(K)
PTOT	Power turbine outlet temperature(K)
S/C	Steam carbon ratio
C	Carbon decomposition rate
ADAM	Adaptive Moment Estimation
RMSE	Root Mean Squared Error
MAE	Mean Absolute Error
MAPE	Mean Absolute Percentage Error
R^2	Multiple determination coefficient

1. INTRODUCTION

With the increasing demand for long-range, high-endurance missions and reliable power performance in large ocean-going vessels, ship propulsion systems are evolving toward greater power density, operational flexibility, and robustness[1]. The adoption of all-electric propulsion systems[2], especially those incorporating hybrid configurations such as IRGT/SOFC, has garnered attention due to their high efficiency (>60%), low noise, and multi-fuel capability[3, 4]. Despite these advantages, dual-unit IRGT/SOFC systems introduce significant modeling and control challenges due to strong nonlinearities, complex thermo-electro-mechanical interactions, and dynamic coupling under varying fuel allocation conditions[5]. Traditional physics-based or single-output data-driven approaches often fail to accurately capture the transient behavior and internal parameter dynamics, particularly when subjected to rapid load fluctuations or dynamic fuel distribution[6]. Prior research has made progress in the modeling and

This is a paper for the 11th Applied Energy Symposium: Low Carbon Cities & Urban Energy Systems (CUE2025), July 18-22, 2025, Kitakyushu, Japan.

performance prediction of single SOFC or SOFC-GT systems. Song et al.[7]used BP neural networks, SVM, and random forest to comparatively predict the performance of SOFC stack, finding that the BP neural network identification method achieved $R^2 > 0.98$ and MAPE < 0.06, validating its effectiveness in SOFC system performance prediction. Wu et al. [8]constructed a biomass gasification gas SOFC-GT integrated system and combined PSO-BP neural networks to predict its performance, analyzing the effects of gasification temperature, S/B ratio, and anode temperature on the system. The calculated results showed R^2>0.98, MAPE<0.06, and RMSE<0.33, verifying the model with high prediction accuracy. Zeng et al.[9] proposed a multi-population PSO-BP neural network dynamic identification model for the dynamic SOFC dry methane reforming system. Using easily measurable inputs such as temperature and fuel flow, to identify difficult-to-measure parameters like the CH_4/CO_2 conversion rate, achieving an average error of less than 5% and R^2>0.97, thereby realizing high-accuracy prediction of the dynamic process. Chen et al. [10] compared unsupervised deep auto-encoder(DAE)-LSTM and LSTM for predicting the dynamic performance of fuel utilization in SOFC-GT hybrid systems. The results showed that the DAE-LSTM model had a maximum error of only 0.00529 and an average error reduced to 0.00025. Recent efforts have shown the potential of artificial neural networks, particularly LSTM architectures, in system identification and prediction for SOFC and hybrid configurations. Nevertheless, most existing studies are limited to single SOFC or SOFC-GT hybrid system, with little attention to dynamic identification modeling of dual-unit systems driven by multiple variables. To address these gaps, this work develops a hybrid modeling approach that integrates physics-based simulations with data-driven LSTM architectures for the dynamic identification and prediction of a dual IRGT-SOFC system. By taking total fuel flow rate and fuel distribution ratio as inputs, the proposed model is capable of real-time prediction of critical system-level outputs including IRGT and SOFC power, SOFC temperature gradient, and efficiency. This approach aims to support real-time adaptive control and power management in next-generation electrified marine platforms operating under dynamic and uncertain conditions.

2. MODELING OF DUAL UNIT IRGT-SOFC SYSTEM

2.1 Topological diagram

A representative 68 MW all-electric ocean-going vessel[11] is selected for modeling and simulation, designed to support a propulsion load of 56 MW and auxiliary high-power electrical loads of 12 MW. As illustrated in Fig. 1, the propulsion system comprises two identical 34 MW hybrid units, each integrating a 24 MW intercooled reheat gas turbine (IRGT) and a 10 MW solid oxide fuel cell (SOFC) stack. Additional subsystems include a pre-reformer (P-R), cracker (CR), catalytic combustion chamber (CCC), heat exchanger (HE), and generator (G). AC outputs from the IRGT are rectified through AC/DC inverters and distributed via a 4 kV DC bus.

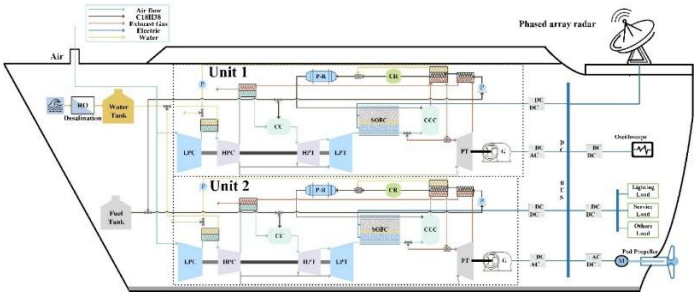

Fig. 1 Structural diagram of all-electric IRGT/SOFC hybrid system on ship

2.2 Data driven hybrid *mathematical* modeling

2.2.1 IRGT dynamic modeling

A data-driven approach based on a three-layer neural network is employed to capture the nonlinear compressor and turbine characteristics. Input-output mapping is performed using historical operational data and experimental maps, as shown in Fig. 2.

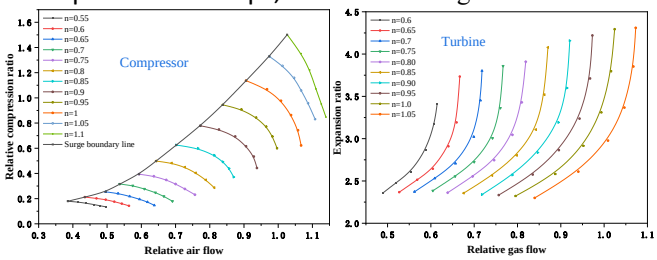

Fig. 2 Compressor and turbine characteristic map

The transient model of the mechanism part has been completed in the previous research[12], mainly including gas outlet temperature, pressure, compressor power consumption, turbine exhaust parameters, and turbine work output.

2.2.2 SOFC dynamic modeling

The model adopts an anode-supported, direct internal reforming SOFC stack design, referencing commercial designs from Bloom Energy[13]. Each stack comprises 450 single cells. The model includes: a thermodynamic sub-model to simulate temperature,

heat and mass transfer. an electrochemical sub-model incorporating polarization, ohmic, and concentration losses. Previous studies from our group provide the basis for this model[14].

2.2.3 Diesel cracking and reforming model

Liquid diesel is selected as the fuel for compatibility with existing marine infrastructure. It is reformed into hydrogen-rich gas using cracking techniques. The complex diesel composition is simplified to $C_{18}H_{38}$ for modeling. This model builds on previous research conducted by our team[15].

2.2.4 Constraint and Design Parameters

The following key constraint conditions need to be considered. The boundary conditions for the model are shown in Table 1[16]. According to selected type ship and above mathematic modeling approach, the main modeling parameters employed in the hybrid system are shown in Table 2.

Table 1 Safety constrains for key components

Parameter	Constraint
Power Turbine Temp. T_{exGT}	<1073K
LPC Surge Margin SM_{LPC}	>10%
SOFC Temp. T_{FC}	<1273
CCC Temp. T_{CCC}	<1473K
SOFC Temp. Gradient T_{FCavg}	<10K/cm
Carbon Deposition Rate C	<5mol/s

Table 2 IRGT/SOFC hybrid system design parameters

Parameters	Value	Parameters	Value
LPC pressure ratio	4.4	Slices/stack	450
HPC pressure ratio	4.55	Stack number	288
Rotor efficiency	99%	S/C	1.54
Inlet air flow rate	104.6kg/s	Current density	5500A/m2
TIT	1550K	SOFC pressure	560kPa
$C_{18}H_{38}$ LHV	47270kJ/kg	Fuel utilization	75%
Anode thickness	0.5mm	Cathode thickness	0.05mm
LPC efficiency	85%	Electrolyte thickness	0.02mm
HPC efficiency	85.8%	Length	0.4m
Volume loss	1-2%	Width	0.1m
HE pressure loss	1-3%	SOFC pressure loss	1-3%
CC, CCC loss	1-5%	Pre-reformer loss	1-5%
Generator efficiency	99%	AC/DC efficiency	99%
Volume	10m^3	Rotor inertia (HP, LP)	200kg/m^2

2.3 Model *Benchmarking*

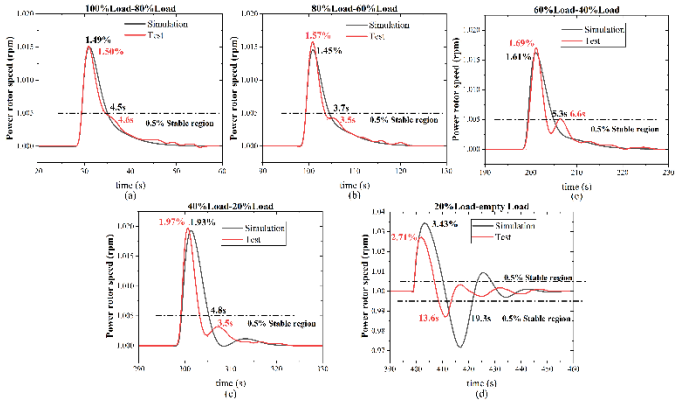

Fig. 3 Simulation and test comparison for PT rotor speed of the gas turbine under load step[12]

The steady state and dynamic benchmark tests of the gas turbine have been completed in the previous research in our group[12]. Steady-state and dynamic validation of the IRGT model demonstrates a maximum rotor overshoot error of only 0.78%, as shown in Fig. 3. The SOFC model is benchmarked using step-change response tests, with transient error within 0.8% as shown in Fig. 4[16], confirming its accuracy.

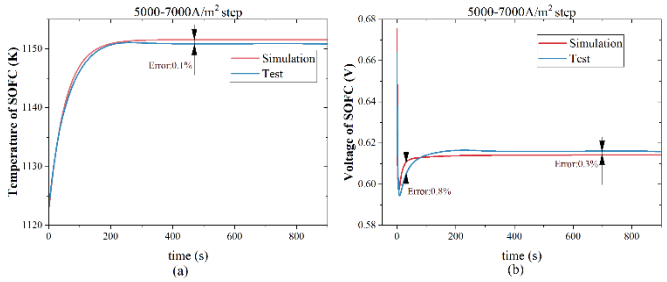

Fig. 4 Transient response of SOFC voltage(a) and temperature output (b) for 5000A/m2 to 7000A/m2[16]

3 IDENTIFICATION MODELING

3.1 MIMO-LSTM Model Structure

To capture the nonlinear and time-dependent behavior of the dual-unit IRGT/SOFC hybrid system, a multi-input multi-output long short-term memory (MIMO-LSTM) neural network is developed. The model inputs include fuel flow rate of each unit. The output layer predicts a set of dynamic parameters, such as SOFC

and IRGT power output, electrical efficiency, SOFC temperature gradient, and carbon deposition rate.

$$u(t) = [G_{fuel}, P_{FC}, P_{GT}, \eta_{ele}, T_{exGT}, T_{FC}, SM_{LPC}, C, T_{FCavg}, T_{ccc}]$$

$$y(t) = [P_{FC}, P_{GT}, \eta_{ele}, T_{exGT}, T_{FC}, SM_{LPC}, C, T_{FCavg}, T_{ccc}]$$

The model structure is shown in the Fig. 5. The main calculation process of LSTM is about forget gate, input gate and output gate computation process, which are shown as below equations from (4) to (9). Among them, σ is the sigmoid activation function. LSTM can effectively handle the temporal dependencies of the system by dynamically updating the cell state c_t and the hidden state h_t through the gating mechanism.

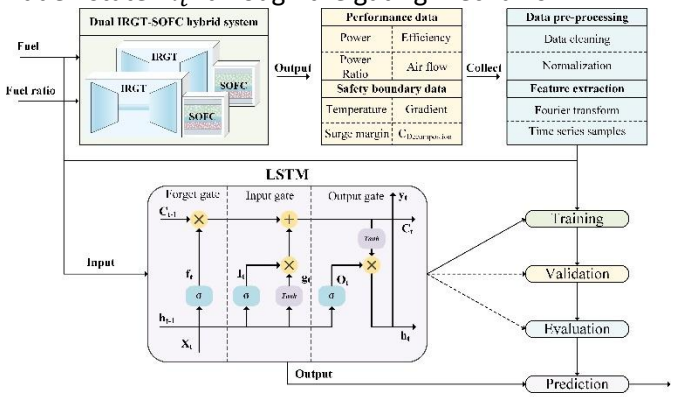

Fig. 5 MIMO-LSTM model structure diagram

$$i_t = \sigma(W_{ii}x_t + b_{ii} + W_{hi}h_i + b_{hi}) \quad (4)$$

$$f_t = \sigma\left(W_{if}x_t + b_{if} + W_{hf}h_{i-1} + b_{hf}\right) \quad (5)$$

$$g_t = tanh\left(W_{ig}x_t + b_{ig} + W_{hg}h_{i-1} + b_{hg}\right) \quad (6)$$

$$o_t = \sigma(W_{io}x_t + b_{io} + W_{ho}h_{i-1} + b_{ho}) \quad (7)$$

$$c_t = f_t \odot c_{t-1} + i_t \odot g_t \quad (8)$$

$$h_t = o_t \odot tanh(c_t) \quad (9)$$

3.2 Data Preprocessing and training

The training dataset is generated by varying fuel flow from 10% to 100% in step-change patterns, using the hybrid simulation model. All input and output variables are normalized to the range [-1, 1] using global Min-Max scaling to reduce unit inconsistency and enhance convergence.

$$x_{norm} = \frac{2(x - x_{min})}{x_{max} - x_{min}} - 1$$

The dataset is randomly split into training (80%), validation (10%), and test (10%) sets. To improve training efficiency and memory utilization, long time series are divided into fixed-length subsequences, forming training samples (XTrain and YTrain)..

$$XTrain_i = \{u_{(i-1)L+1}, u_{(i-1)L+2} \dots u_{iL}\}$$

The network is trained using the ADAM optimizer with a learning rate set to 1 initially, and the mean squared error as the loss function. Table 3 summarizes the key network settings.

Table 3 MIMO-LSTM Hyperparameter Settings

Category	Name	Value
Structure	Input layer neurons number	10
	Fully connected layer neurons number	9
	Hidden layer number	1, 2
	Hidden layer neurons number	25, 50, 100
Training	Length of sequence	2000
	Maximum training epochs	100
	Batch size	64
	Optimizer	ADAM
	Cost function	MSE

4 RESULTS AND DISCUSSION

4.1 Impact of Sampling Time on Prediction Accuracy

Table 4 Performance index under different sample time

Index	Sample time 0.001s		Sample time 0.01s		Sample time 0.1s	
	P_{FC}	P_{GT}	P_{FC}	P_{GT}	P_{FC}	P_{GT}
RMSE	13kW	6kW	21 kW	34 kW	163 kW	336 kW
MAE	11kW	5kW	16 kW	8 kW	59 kW	80 kW
MAPE	0.11%	0.09%	0.15 %	0.30 %	0.75 %	1.79 %
R^2	99.9%	99.9%	99.9%	99.9%	99.7%	99.6%
Spent	776 minutes Memory 90GB		30 minutes Memory 40GB		2 minutes Memory 25GB	

The influence of sampling intervals (0.001 s, 0.01 s, and 0.1s) on model performance was evaluated. As shown in Table 4, longer sampling intervals result in degraded prediction accuracy. For example, when the sample time increased from 0.001 s to 0.1 s, the RMSE for SOFC power rose from 13 kW to 163 kW, and the RMSE for GT power increased from 6 kW to 336 kW. MAPE values also increased, confirming the negative impact of reduced data resolution.

However, smaller time steps significantly increase computational costs. Training with a 0.001 s sample time required 776 minutes and 90 GB of memory, compared to only 2 minutes and 25 GB for the 0.1 s case. Thus, a sample time of 0.01 s was chosen as the optimal balance between precision and computational efficiency.

4.2 Effect of *Hidden* Layer Depth

To assess the effect of network depth, LSTM models with one and two hidden layers (100 neurons each) were compared. Results in Table 5 show that increasing the

layer number slightly reduces R² values for some outputs and significantly increases prediction error for SOFC temperature gradient, where the MAE increased from 0.01 K to 0.11 K and MAPE rose from 1.4% to 13.2%. Meanwhile, computational cost rose by 80% in time and 24% in memory. These findings suggest that a deeper network does not guarantee better performance and may even hinder generalization due to overfitting in complex multi-output tasks.

Table 5 LSTM performance under different hidden layer

Index	One layer			Two layers		
	MAE	MAPE	R^2	MAE	MAPE	R^2
P_{FC}	38kW	0.4%	99.9%	38kW	0.66%	99.8%
P_{GT}	47kW	0.6%	99.9%	59kW	1.10%	99.9%
η_{ele}	0.25%	0.45%	99.9%	0.2%	0.46%	99.2%
T_{exGT}	0.6K	0.06%	99.9%	3.9K	0.41%	99.7%
T_{FC}	1.12K	0.09%	99.9%	2.88K	0.24%	99.8%
SM_{LPC}	0.007	0.89%	100%	0.011	1.64%	99.9%
C	0.012	0.37%	99.9%	0.016	0.70%	99.7%
T_{FCavg}	0.01	1.4%	99.9%	0.11	13.2%	97.7%
T_{ccc}	1.2K	0.08%	99.9%	4.75K	0.33%	99.7%
Spent	34min 45GB			62min 56GB		

4.3 Influence of Neuron Count

Models with 25, 50, and 100 neurons per hidden layer were evaluated. As shown in Table 6, 50 neurons achieved the best balance of accuracy. Compared to the 25-neuron model, the 50-neuron network reduced MAE by over 60% for critical outputs such as SOFC power and temperature. Increasing to 100 neurons caused degradation in some performance metrics, possibly due to overfitting or insufficient training data volume.

Table 6 Performance under different neurons number

Index	Neurons number:50			Neurons number:25		
	MAE	MAPE	R^2	MAE	MAPE	R^2
P_{FC}	14kW	0.19%	99.9%	36kW	0.46%	99.9%
P_{GT}	15kW	0.26%	100%	19kW	0.37%	100%
η_{ele}	0.1%	0.22%	99.9%	0%	0.17%	99.8%
T_{exGT}	1.38K	0.15%	99.9%	0.97K	0.10%	99.9%
T_{FC}	1.32K	0.11%	99.9%	0.26K	0.02%	99.9%
SM_{LPC}	0.002	0.79%	100%	0.001	0.31%	100%
C	0.006	0.21%	99.9%	0.017	0.58%	99.9%
T_{FCavg}	0.034	2.73%	99.8%	0.046	3.46%	99.8%
T_{ccc}	0.72K	0.05%	99.9%	0.59K	0.04%	99.9%

4.4 Sensitivity to Learning Rate

Further tests were conducted to analyze precision with learning rates of 0.01 and 0.0001. The highest learning rate of 0.01 resulted in comparatively larger prediction errors, as evidenced by increased MAE and MAPE values across most parameters. Conversely, the lowest learning rate of 0.0001 yielded reduced MAE; however, it exhibited higher MAPE than the 0.001 rate in critical metrics such as P_{FC} and T_{FCavg}.The learning rate of 0.001 demonstrated superior performance, achieving significantly lower MAPE values, exceeding a 60% reduction in T_{FCavg} compared to 0.01. Therefore, the learning rate of 0.001 is identified as optimal.

Table 7 Performance index under different learning rate

Index	Learning rate:0.01			Learning rate:0.0001		
	MAE	MAPE	R^2	MAE	MAPE	R^2
P_{FC}	57kW	0.76%	99.9%	11kW	0.35%	99.9%
P_{GT}	50kW	0.72%	99.9%	40kW	0.76%	99.9%
η_{ele}	0.4%	0.85%	99.7%	0.1%	0.19%	99.7%
T_{exGT}	1.35K	0.14%	99.9%	0.44K	0.04%	99.9%
T_{FC}	2.15K	0.18%	99.9%	0.82K	0.07%	99.9%
SM_{LPC}	0.004	0.74%	100%	0.003	0.70%	99.9%
C	0.036	1.39%	99.8%	0.008	0.32%	99.9%
T_{FCavg}	0.083	7.37%	99.6%	0.045	3.74%	99.4%
T_{ccc}	5.68K	0.40%	99.8%	0.66K	0.04%	99.9%

These results not only confirm the high numerical accuracy presented in previous subsections but also emphasizes the practical interpretability and engineering relevance of the LSTM-based dynamic identification approach.

5 CONCLUSIONS

This study developed and validated a high-fidelity dynamic prediction model for a dual-unit IRGT/SOFC hybrid marine propulsion system using a multi-input multi-output long short-term memory network. By integrating mechanism-based hybrid simulations with deep learning techniques, the model achieved high accuracy in forecasting key performance indicators, including power output, thermal responses, and fuel efficiency under varying operational conditions. Key conclusions include:

1) Sampling rate strongly affects both accuracy and computational efficiency. Therefore, a sample time of 0.01 s is selected as the optimal compromise, offering high predictive accuracy (MAPE < 0.3%) with reasonable computational cost.

2) A single hidden layer with 50 neurons demonstrated the best trade-off between global performance and local mutation error. It reduced the MAE for SOFC power from 36 kW to 14 kW, and for GT power from 19 kW to 15 kW. Additionally, MAPE for electrical efficiency was as low as 0.22%.

3) The final LSTM model achieved R^2 values exceeding 0.998 across all key outputs, with MAPE consistently below 0.79% except T_{FCavg}. Furthermore, real-time validation under dynamically varying fuel

distributions demonstrated the model's ability to accurately track both steady-state and transient behaviors with minimal lag and low computational overhead.

Above results affirm the potential of the proposed MIMO-LSTM architecture as a real-time predictive control module for next-generation marine propulsion systems in complex operational scenarios.

ACKNOWLEDGEMENT

The research is supported by National Natural Science Foundation of China under Grant No. (52176013), Shanghai Inter-governmental International Cooperation Project No. (23160710200), National Science and Technology Major Project (J2019-I-0012-0012). And by the UK Royal Society under Grant IES\R3\213195.

REFERENCE

[1]D. T. N. a. D. A. P. Dr. Jean-Paul Rodrigue. "Ports, Maritime Shipping and International Trade." https://porteconomicsmanagement.org/pemp/contents/part1/maritime-shipping-and-international-trade/ (accessed.

[2]G. Rigatos, M. A. Hamida, M. Abbaszadeh, and P. Siano, "A nonlinear optimal control approach for shipboard AC/DC microgrids," *Electric power systems research,* vol. 209, p. 108024, 2022, doi: 10.1016/j.epsr.2022.108024.

[3]X. Lv, P. Hong, J. Wen, Y. Ma, C. Spataru, and Y. Weng, "Highly efficient operation of an innovative SOFC powered all-electric ship system using quick approach for ammonia to hydrogen," *Frontiers in Energy,* 2025/01/01 2025, doi: 10.1007/s11708-025-0974-8.

[4]P. Kumar and O. Singh, "A review of solid oxide fuel cell based hybrid cycles," *International journal of energy research,* no. 7, p. 46, 2022.

[5]Z. Guo *et al.*, "Intelligent Digital Twin Modelling for Hybrid PV-SOFC Power Generation System," *Energies (Basel),* vol. 16, no. 6, p. 2806, 2023, doi: 10.3390/en16062806.

[6]S. S. Blakseth, A. Rasheed, T. Kvamsdal, and O. San, "Combining physics-based and data-driven techniques for reliable hybrid analysis and modeling using the corrective source term approach," *Applied soft computing,* vol. 128, no. C, p. 109533, 2022, doi: 10.1016/j.asoc.2022.109533.

[7]S. Song, X. Xiong, X. Wu, and Z. Xue, "Modeling the SOFC by BP neural network algorithm," *International journal of hydrogen energy,* vol. 46, no. 38, pp. 20065-20077, 2021, doi: 10.1016/j.ijhydene.2021.03.132.

[8]X.-l. Wu *et al.*, "Performance prediction of gasification-integrated solid oxide fuel cell and gas turbine cogeneration system based on PSO-BP neural network," *Renewable energy,* vol. 237, p. 121711, 2024, doi: 10.1016/j.renene.2024.121711.

[9]S. Zeng *et al.*, "Electrochemical promoted dry methane reforming for power and syngas co-generation in solid oxide fuel cells: Experiments, modelling and optimizations," *International journal of hydrogen energy,* vol. 50, pp. 1220-1231, 2024, doi: 10.1016/j.ijhydene.2023.10.151.

[10]J. Chen, Y. Chen, and H. Zhang, "Study on Fuel Utilization Dynamic model of a SOFC-GT Hybrid System Based on Deep Learning Technique," *E3S web of conferences,* vol. 113, p. 2010, 2019, doi: 10.1051/e3sconf/201911302010.

[11]https://military-history.fandom.com/wiki/Type_052D_destroyer. "Type 052D destroyer." https://military-history.fandom.com/wiki/Type_052D_destroyer (accessed.

[12]J. Wen, S. Zhang, J. Lu, C. Spataru, Y. Weng, and X. Lv, "Coordinated intelligent control strategy and power management for marine gas turbine under pulsed load using optimized neural network," *Energy,* p. 133719, 2024/11/08/ 2024, doi: https://doi.org/10.1016/j.energy.2024.133719.

[13]B. energy. "Load Following Solid Oxide Fuel Cell " https://www.bloomenergy.com/wp-content/uploads/load-following-solid-oxide-fuel-cell.pdf (accessed.

[14]X. Wang, X. Mi, X. Lv, and Y. Weng, "Fast and stable operation approach of ship solid oxide fuel cell-gas turbine hybrid system under uncertain factors," *International journal of hydrogen energy,* vol. 47, no. 50, pp. 21472-21491, 2022, doi: 10.1016/j.ijhydene.2022.04.284.

[15]X. Mi, J. Wen, J. Yang, C. Spataru, Y. Weng, and X. Lv, "Safety and fast-tracking assessment of an innovative SOFC/GT all-electric ship propulsion system under pulsed load," *Applied Thermal Engineering,* vol. 270, p. 126246, 2025/07/01/ 2025, doi: https://doi.org/10.1016/j.applthermaleng.2025.126246.

[16]P. Aguiar, C. S. Adjiman, and N. P. Brandon, "Anode-supported intermediate-temperature direct internal reforming solid oxide fuel cell - II. Model-based dynamic performance and control," *J POWER SOURCES,* vol. 147, no. 1-2, pp. 136-147, 2005, doi: 10.1016/j.jpowsour.2005.01.017.